EUROPEAN ORGANIZATION FOR NUCLEAR RESEARCH

to the ISOLDE and Neutron Time-of-Flight Committee

Local study of Lithium Niobate domain walls

9th of April 2024

J. H.-Schell[1,2], H. M. Gürlich[3], T. T. Dang[2], I. C. J. Yap[2], B. Dörschel[2], S. D. Seddon[3], B. Koppitz[3], A. M. L. Lopes[4], A. W. Carbonari[5], N. Lima[1,5], P. Rocha-Rodrigues[4], L. M. Eng[3,6]

[1] *European Organization for Nuclear Research (CERN), CH-1211 Geneva, Switzerland*
[2] *Institute for Materials Science and Center for Nanointegration Duisburg-Essen (CENIDE), University of Duisburg-Essen, 45141 Essen, Germany*
[3] *Institute of Applied Physics, Technische Universität Dresden, 01062 Dresden, Germany*
[4] *Institute of Physics for Advanced Materials, Nanotechnology and Photonics (IFIMUP), 4169 - 007 Porto*
[5] *Instituto de Pesquisas Energéticas e Nucleares IPEN-CNEN/SP, São Paulo 05508-000, Brazil*
[6] *ct.qmat: Dresden-Würzburg Cluster of Excellence—EXC 2147, Technische Universität Dresden, 01062 Dresden, Germany*

Spokesperson: Juliana H.-Schell (juliana.schell@cern.ch), Lukas M. Eng (lukas.eng@tu-dresden.de)
Contact person: Juliana H.-Schell (juliana.schell@cern.ch)

CERN-INTC-2024-034 / INTC-P-703
09/04/2024

Abstract: We propose the study of the $LiNbO_3$ (LNO) materials family via perturbed angular correlations at ISOLDE-CERN. Single domain poled and periodically poled LNO samples are to be investigated upon different annealing and temperature conditions after the implantation of the ^{111m}Cd probe at 30 keV. The goal is to investigate the anomalies observed in the perturbation functions of periodically poled single crystals and correlate the results with: (I) a possible local conductivity effect on the domain walls; and (II) the second-Harmonic-Generation polarimetry parameters. The proposed measurements associated with density functional theory can provide insight into the mechanisms of electron transport and charge trapping in charged LNO domain walls and support their use in prospective nanoelectronic devices.

Summary of requested shifts: 12 shifts of protons on target, (split into at least 3 runs over 2024 and 2025)

1 Motivation

A prominent scientific challenge to obtain renewable energy-harvesting solutions for a sustainable future requires the investigation of materials functionalities down to the atomic scale. For instance, the potential application of ferroelectric materials in photovoltaics has attracted much attention, since certain materials can display remarkable photovoltages and spontaneous photocurrents [1, 2]. Since the '70s the photovoltaic effect has been investigated [3-7] in the lithium niobate (LNO) family, and this became one of the most explored ferroelectric materials. It is well known that small amounts of certain dopants, such as magnesium, increase the resistance against optical damage in LNO. The 5-%Mg doping level leads to a two-order higher optical stability while other characteristics like the piezoelectric coefficients are only slightly changed [8].

The new nanoelectronics field, in which the domain wall in ferroic materials is itself an active device element and the investigation of local properties in the domain walls became crucial to support the ability to spatially modulate the ferroic order parameter within a single domain wall [9, 10]. Domain walls are classified as a topological defect and can be found in ordered crystal structures such as in LNO samples. Moreover, it has been observed that charged ferroelectric domain walls (CDW) [11] in LNO have a 13-order higher conductivity than in LNO bulk [12]. In the scope of this discovery, it is proposed that a new generation of adaptive-optical elements, such as electrically controlled integrated-optical chips for quantum photonics, and advanced LN-semiconductor-hybrid optoelectronic devices may be created [12].

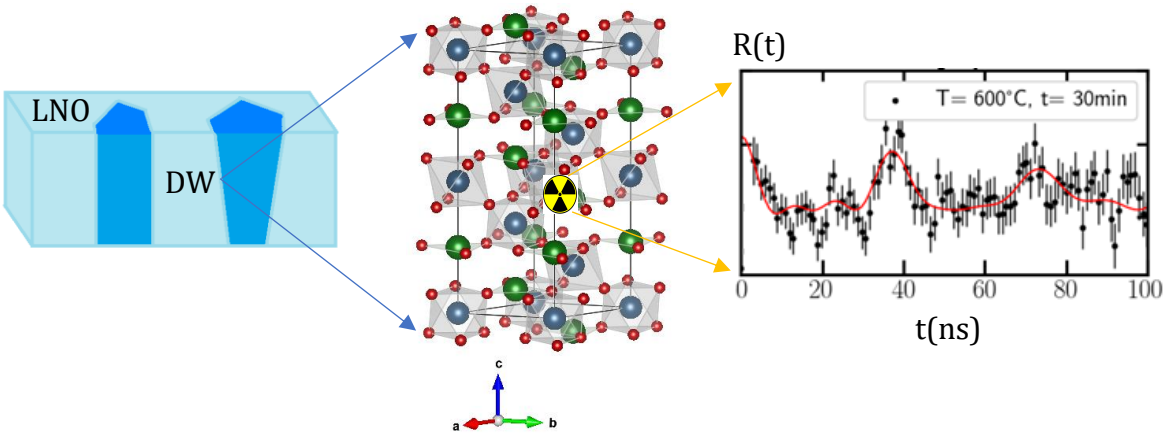

Figure 1: *Representation of three-dimensional domain wall (DW) profile in the LNO single crystal zoomed in on the ^{111m}Cd-implanted trigonal crystal lattice structure and the obtained perturbation function R(t).*

Furthermore, local slopes of CDW were observed and tracked across entire ferroelectric LNO single crystals [13] using the Cherenkov second-harmonic generation, which is a technique for three-dimensional domain wall profiling in the entire crystal. The time-differential perturbed angular correlation (TDPAC) technique [14-16] can complement the information obtained by this technique with the determination of the local

extranuclear fields and charge distribution in the vicinity of the TDPAC probe (schematic of Figure 1). Moreover, the pathway of LNO DW can be determined with high resolution using optical and interferometric approaches [17] before and after the TDPAC experiments. A comprehensive study of the electrical-transport mechanism in 5% MgO-doped LNO reported on the temperature-dependent current-voltage curves and the subsequent physical parameters relevant to the main mechanisms of ferroelectric DW [18]. The electrical impedance properties of the CDW were investigated on the nanometre-length scale and the hopping of excited charge carriers along the CDW was identified as the dominant charge transport process [19]. To complement these studies, we therefore propose to measure the room-temperature current-voltage characteristics during the TDPAC measurements and compare the obtained results with conventional TDPAC experiments.

B. Hauer et al. (1995) [20] reports on the temperature dependence of the hyperfine parameters of 5%Mg-doped and undoped LNO via TDPAC using ^{111m}Cd at ISOLDE-CERN or ^{111}In as a probe. The study includes the temperature dependence of the electrical field gradient (EFG). Annealing for 30 min at 600 °C was found to be sufficient to repair the damages caused by the ion-implantation process of ^{111m}Cd at 60 keV. Using the point charge model, the authors concluded that the implanted Cadmium or Indium is positioned at the Lithium-site. The results show that Mg doping at 6 mol % does not have any effect on the lattice location of these impurities in LNO. However, no density functional theory (DFT) calculations were performed to additionally confirm this. Therefore, these simulations are part of our work and will support the data interpretation to understand the local CDW or DW effects.

Y. Ohkubo et al. in 2002 [21, 22] used ^{111m}Cd and ^{117}In as TDPAC probes to study high-purity pellets of $LiTaO_3$ (LTO) doped with In and Cd and associate the results with the LTO-LNO system. The results indicate that the order-disorder of oxygen ions is the driving mechanism for ferroelectric instability in the $LiNbO_3$–$LiTaO_3$ system. The values of this study for the EFG at the Li-site were found to be ω = 223(1) Mrad/s at T = 77 K. This value differs from the values found by B. Hauer et al. [20] for LNO. Nevertheless, similar temperature dependencies were found in both crystal structures. The EFG does only change slightly in both types (up to 10 %) when changing the temperature in the range of 77 K to around 600 K. This is of fundamental help, as the first principles DFT calculations are performed for 0 K and thus knowing the temperature dependency helps comparing the DFT results to the experimental results.

2 Methodology

Experimental

The proposed time-differential perturbed angular correlation experiments (TDPAC) [14-16] will be conducted after the ion-implantation of ^{111m}Cd probe at 30 keV into LNO

samples. Preliminary TDPAC measurements were carried out in (5% Mg-doped) LNO single crystals after different annealing conditions. Two kinds of polarized crystals were used; (I) in z-direction polarized single domain crystals, and (II) in z-direction periodically poled. In the single domain crystal, there are no domain walls as only one polarization direction exists. We investigated the evolution of the implantation damage recovery after thermal treatments at 600 °C, 700 °C or 800 °C for 20 or 30 minutes under O_2 flow. The subsequent TDPAC experiments were conducted in air with the Raghavan geometry at room temperature using a four-detectors setup [16] and the obtained spectra can be found in Figure 2.

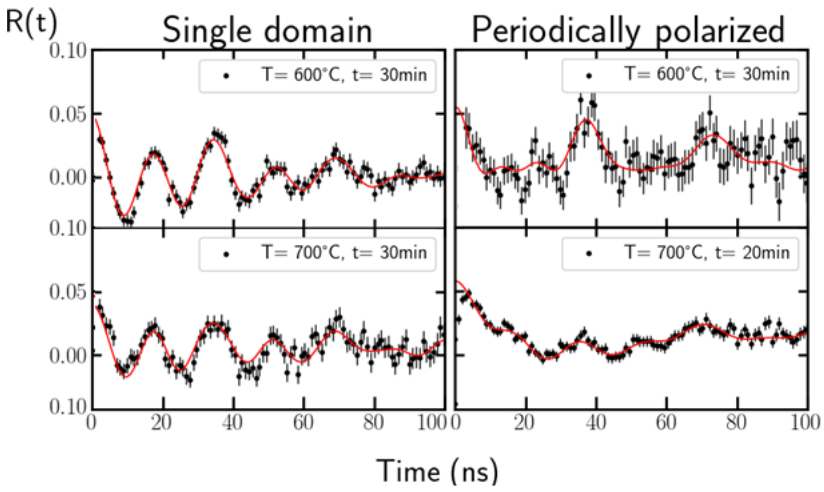

Figure 2: *TDPAC spectra of 5% Mg-doped LNO single crystals measured at room temperature after the ^{111m}Cd implantation and annealing.*

Due to the very low concentration of the ^{111m}Cd or ^{111}In nuclear probes used in a TDPAC experiment, the tracer ions represent only a weak dopant and do not influence the overall properties of the LNO solid. A great advantage of TDPAC in comparison to other hyperfine techniques is that it can be performed in a wide temperature range, even at temperatures up to and beyond the melting point of materials, without affecting the quality of the TDPAC signal. The obtained hyperfine parameters are promising to study DW effects at the local scale as can be seen in Figure 3. Observable changes in R(t) spectra measured with the periodically poled sample implies different hyperfine parameters, with much lower values for the electric quadrupole frequencies, and showing evidence of dynamic effect on the quadrupole interactions.

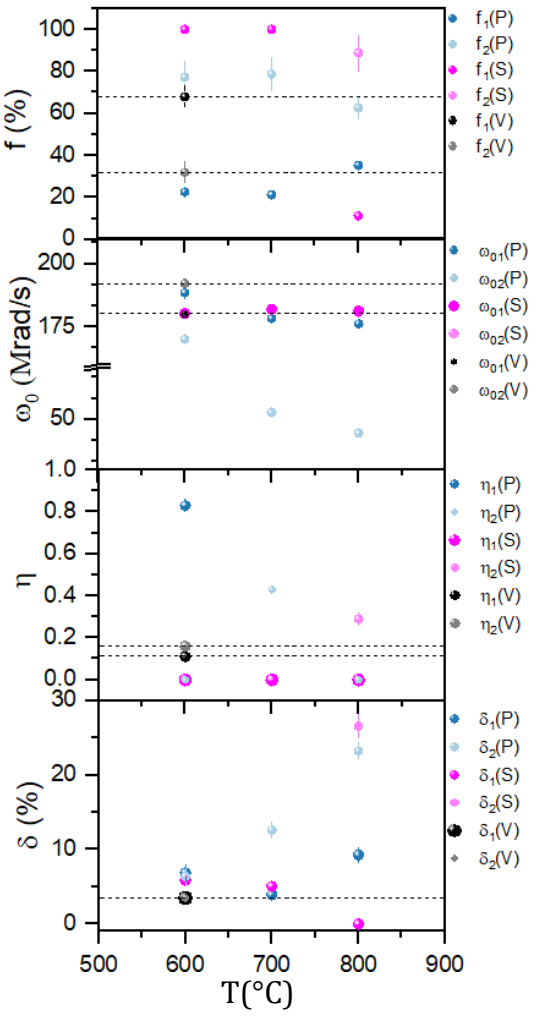

Figure 3: *Hyperfine parameters as a function of annealing temperature (T). These were obtained at room temperature after the implantation of ^{111m}Cd at 30 keV in LNO single domain (S) or periodically poled (P) LNO. Data points (V) from the reference [20] are displayed with dashed lines for a better comparison.*

The site one for single domain samples presents electric quadrupole frequencies (ω_0) values, that are very close to the values reported in the literature [20], and therefore confirm the reproducibility of the experiment. Moreover, the low values of the asymmetry parameter (η) obtained for the single domain condition are also compatible with the work of B. Hauer et al. (1995) [20].

Two fraction (f) sites for the Cd probe were observed in periodically poled samples. Obviously, not all probes are located in the DW, but the effect of polarization is clearly observable.

Simulations

For the simulation of the ^{111m}Cd substitution at the Li site of LNO, we performed ab-initio Density Functional Theory (DFT) calculations using the Vienna Ab Initio Simulation Package (VASP) program [23], based on the projector augmented wave (PAW) [24]. The calculation of the EFG of the Cd ion, that VASP uses, is based on its surrounding electron density using the PAW formalism and associated with the work of Helena Petrilli et al. [25]. We used the PBE91 exchange correlational functional in the framework of the generalized gradient approximation (GGA) [26]. We performed both electronic and ionic relaxation of the LNO atoms and used the atomic PAW potentials available in VASP [27] for Li, Ni and O atoms. The valence of these PAW potentials is 3, 13 and 6 respectively, corresponding to the $1s^2 2s^1$, $4s^2 4p^6 4d^4 5s^1$ and $2s^2 2p^4$ energy levels of neutral Li, Ni and O, as the EFG is sensitive to the inclusion of the so-called semi-core states as valence electrons [25].

For the Cd(LNO) defect calculations, from our converged pure LNO calculations, we created a 2 by 2 by 2 supercell, which allows the mirror Cd atoms to be more than 1 Å away from each other, to avoid interaction between Cd atoms. The PAW potential used

for the Cd atom is Cd_sv_GW, which has 20 valence electrons and corresponds to $4s^2 4p^6 4d^{10} 5s^2$ energy levels of neutral Cd. We have also performed calculations where 2) the oxidation state of Cd is +1, and 3) the oxidation state of Cd is +2, and we introduced one Li vacancy. In the Table 1, we compare our results against that of [20]. We note that our diagonalized EFG values of the Cd_{Li} atom are close to the experimental results obatined by [20]. Considering the Li vacancy as the nearest neighbor, we can see that the asymmetry parameter, as reported by our DFT system, is close with that of [20]. The asymmetry parameter of the Cd_{Li} site is preserved if we do not allow for any vacancy formation.

System	Charge of System	$V_{33}^{DFT}(V/A^2)$	η^{DFT}	$\Delta H^{DFT}(eV)$	$\omega_0^{DFT}[Mrad/s]$
Cd_{Li}	+1	90.956	0.000	-1.9529	172(1)
Cd_{Li}	0	89.243	0.000	4.8395	168(1)
Cd_{Li} with Li vacancy	0	91.726	0.106	8.5434	173(1)
		$V_{33}^{Exp}(V/A^2)$	η^{Exp}		$\omega_0^{Exp}[Mrad/s]$
Present study (*Single domain, T = 600 °C*)	-	95.3(4)	0	-	180.4(7)
Present study (*Single domain, T = 700 °C*)	-	96.2(1)	0	-	182(1)
[20] site 1	-	93.9(1)	0.11(2)	-	180(1)
[20] site 2	-	98.8(2)	0.16(4)	-	192(1)

Table 1: Relevant parameters for the Cd(LNO) calculation (^{DFT}) and experimental values (^{Exp}). Note that the reported values in $\Delta H^{DFT}(eV)$ are taken with reference to the equivalent LNO supercell system without any defects.

In summary, our experimental tests could reproduce the experimental results obtained previously [20] for single domain LNO and the extracted EFG parameters are close to the ones obtained by the DFT simulations for the same physics case. However, there is still a lot of open questions to understand the data of periodically poled samples. Due to the LNO complexity, we must investigate which defects and DW effects play an important role. Consequently, we propose to continue the experiments systematically in order to better understand the local effects and how they are related to the charge transport properties in DW and CDW LNO.

References

[1] K. Butler, J. Frost, A. Walsh, Energy Environ. Sci. 8 (2015) 838.

https://doi.org/10.1039/C4EE03523B

[2] Y. Yuan, Z. Xiao, B. Yang, J. Huang, J. Mater. Chem. A 2 (2014) 6027.
https://doi.org/10.1039/C3TA14188H
[3] L. Arizmendi, Phys. Status Solidi A 201 (2004) 253.
https://doi.org/10.1002/pssa.200303911
[4] A. M. Glass , D. Von der Linde and T. Negran, Appl. Phys. Lett., 25 (1974) 233.
https://doi.org/10.1063/1.1655453
[5] J. Carnicero , O. Caballero , M. Carrascosa and J. Cabrera , *Appl. Phys. B*, 79 (2004) 351. https://doi.org/10.1007/s00340-004-1543-1
[6] B. Kang et al. Opt. Commun. 266 (2006) 203.
https://doi.org/10.1016/j.optcom.2006.04.064
[7] J. Spanier et al. Nat. Photon. 10 (2016) 688.
https://doi.org/10.1038/nphoton.2016.188
[8] Y. Furukawa et al., Jpn. J. Appl. Phys. 35 (1996) 2740.
https://dx.doi.org/10.1143/JJAP.35.2740
[9] R. K. Vasudevan et al., Nano Lett. 12, 11, (2012) 5524.
https://doi.org/10.1021/nl302382k
[10] G. Catalan, J. Seidel, R. Ramesh, J. F. Scott, Rev. Mod. Phys. 84 (2012) 119.
https://doi.org/10.1103/RevModPhys.84.119
[11] R. K. Vasudevan, et al. Adv. Funct. Mater. 23 (2013) 2592.
https://doi.org/10.1002/adfm.201300085
[12] C. S. Werner et al., Scientific Reports 7 (2017) 9862.
https://doi.org/10.1038/s41598-017-09703-2.
[13] T. Kämpfe et al., Phys. Rev. B 89 (2014) 035314.
https://doi.org/10.1103/PhysRevB.89.035314
[14] A. Abragam and R. V. Pound, Physical Review 92, 943 (1953).
https://doi.org/10.1103/PhysRev.92.943
[15] G. Schatz, A. Weidinger. Nuclear Condensed Matter Physics, Wiley, Chichester (1996). 6978-0-471-95479-8 (ISBN).
[16] J. Schell, P. Schaaf, and D. C. Lupascu. AIP Advances 7, 105017 (2017).
https://doi.org/10.1063/1.4994249
[17] T. Kämpfe et al., Appl. Phys. Lett. 107 (2015) 152905.

https://doi.org/10.1063/1.4933171

[18] M. Zahn et al., Phys. Rev. Applied 21 (2024) 024007.

https://doi.org/10.1103/PhysRevApplied.21.024007

[19] M. Schröder et al., Mater. Res. Express 1, 035012 (2014).

https://doi.org/10.1088/2053-1591/1/3/035012

[20] B. Hauer et al., Phys. Rev. B, Condensed matter 51 (1995) 6208.

https://doi.org/10.1103/PhysRevB.51.6208

[21] Y. Ohkubo et al. Materials Transactions 43 (2002) 1469.

https://doi.org/10.2320/matertrans.43.1469

[22] Y. Ohkubo et al. Phys. Rev. B 65 (Jan. 2002).

https://doi.org/10.1103/PhysRevB.65.052107

[23] G. Kresse, J. Furthmüller, Phys. Rev. B, Condensed Matter 54 (1996) 11169.

https://doi.org/10.1103/physrevb.54.11169

[24] P. E. Blöchl, Phys. Rev.. B, Condensed Matter 50 (1994) 17953.

https://doi.org/10.1103/physrevb.50.17953

[25] H. M. Petrilli, P. E. Blöchl, P. Blaha, K. Schwarz, Phys. Rev. B, Condensed Matter 57 (1998) 14690. https://doi.org/10.1103/physrevb.57.14690

[26] J. P. Perdew, K. Burke, M. Ernzerhof, Phys. Rev. Lett. 77 (1996) 3865.

https://doi.org/10.1103/physrevlett.77.3865

[27] G. Kresse, D. P. Joubert, Phys. Rev. B, Condensed Matter 59 (1999) 1758.

https://doi.org/10.1103/physrevb.59.1758

3 Details for the Technical Advisory Committee

3.1 General information

Describe the setup which will be used for the measurement. If necessary, copy the list for each setup used.

☒ Permanent ISOLDE setup: SSP chamber at the GLM beam line (170/R-026), KATAME and PACBIT spectrometers (508/R-008),

fume-hoods (GLM area 170/R-026 and chemical laboratory 508/R-002), annealing furnaces at 508/R-004.

☒ To be used without any modification

☐ To be modified: *Short description of required modifications.*

☐ Travelling setup (*Contact the ISOLDE physics coordinator with details.*)

☐ Existing setup, used previously at ISOLDE: *Specify name and IS-number(s)*

☐ Existing setup, not yet used at ISOLDE: *Short description*

☐ New setup: *Short description*

3.2 Beam production

- Requested beams:

Isotope	Production yield in focal point of the separator (/μC)	Minimum required rate at experiment (pps)	$t_{1/2}$
^{111}In	1.10^{6} /μC		2.8 days
^{111m}Cd	1.10^{8} /μC	The following information could be useful: 800E^{10} ppp (source ISO_GPS logbook 20-09-2023 15:00:39) with equidistant pulses. STAGISO, proton current between 0.25 and 0.50 uA expected	49 min

- Full reference of yield information: target group was consulted.
- Target - ion source combination:

  Target UC_x and ion source hot plasma for ^{111}In.

  Target molten Sn with VADIS ion source for ^{111m}Cd.

- RILIS? *No*

☐ Special requirements: (*isomer selectivity, LIST, PI-LIST, laser scanning, laser shutter access, etc.*)

- Additional features?

  ☐Neutron converter: (*for isotopes 1, 2 but not for isotope 3.*)

  ☐ Other: (*quartz transfer line, gas leak for molecular beams, prototype target, etc.*)

- Expected contaminants: *No contaminants expected.*
- Acceptable level of contaminants: As low as possible (materials are sensitive to contaminants)
- Can the experiment accept molecular beams? No.
- Are there any potential synergies (same element/isotope) with other proposals and LOIs that you are aware of? LOI248, LOI249, IS713, IS730, IS732, IS738. Our experiment can be schedule together with these proposals without any issues.

3.3 HIE-ISOLDE

For any inquiries related to this matter, reach out to the ISOLDE machine supervisors (please do not wait until the last minute!).

- HIE ISOLDE Energy: *(MeV/u); (exact energy or acceptable energy range)*

  ☐ Precise energy determination required

  ☐ Requires stable beam from REX-EBIS for calibration/setup? *Isotope?*

- REX-EBIS timing

  ☐Slow extraction

  ☐ Other timing requests

- Which beam diagnostics are available in the setup?
- What is the vacuum level achievable in your setup?

3.4 Shift breakdown

The beam request only includes the shifts requiring radioactive beam, but, for practical purposes, an overview of all the shifts is requested here. Don't forget to include:

- Isotopes/isomers for which the yield need to be determined
- Shifts requiring stable beam (indicate which isotopes, if important) for setup, calibration, etc. Also include if stable beam from the REX-EBIS is required.

An example can be found below, please adapt to your needs. Copy the table if the beam time request is split over several runs.

Summary of requested shifts:

With protons	Requested shifts
Yield measurement of isotope 1	
Optimization of experimental setup using isotope 2	
Data taking, isotope 1	^{111}In: 2 shifts
Data taking, isotope 2	^{111m}Cd: 10 shifts
Data taking, isotope 3	
Calibration using isotope 4	
Without protons	Requested shifts
Stable beam to GLM	1 shift of ^{40}Ar,

3.5 Health, Safety and Environmental aspects

3.5.1 Radiation Protection

• If radioactive sources are required:

  - Purpose? Perturbed angular correlation experiments.
  - Isotopic composition? ^{111m}Cd or ^{111}In.
  - Activity? 2.6x10^{6} Bq (^{111m}Cd) or ^{111}In (2x10^{8} Bq).
  - Sealed/unsealed? Unsealed.

• For collections:

- Number of samples? 50
- Activity/atoms implanted per sample? Maximum $2x10^{11}$ atoms per sample.
- Post-collection activities? *handling, annealing and measurements. Shipping of non-radioactive samples to the home institution*

3.5.2 Only for traveling setups

- Design and manufacturing

☐ Consists of standard equipment supplied by a manufacturer

☒ CERN/collaboration responsible for the design and/or manufacturing

- Describe the hazards generated by the experiment:

Domain	Hazards/Hazardous Activities		Description
Mechanical Safety	Pressure	☒	Gas bottles (200 bar – 10 liters) of Oxygen, Argon or Nitrogen for the annealing. Quantity used: 1 cm^3/s during annealing.
	Vacuum	☒	SSP chamber 10^{-6} mbar
	Machine tools	☐	
	Mechanical energy (moving parts)	☐	
	Hot/Cold surfaces	☐	
Cryogenic Safety	Cryogenic fluid	☐	[fluid] [m3]

Electrical Safety	Electrical equipment and installations	☒	230 V: KATAME and PACBIT spectrometers (508/R-008), SSP chamber at the GLM beam line (170/R-026), fume-hoods (GLM area 170/R-026 and chemical laboratory 508/R-002), annealing furnaces at 508/R-004.

	High Voltage equipment	☐	[voltage] [V]
Chemical Safety	CMR (carcinogens, mutagens and toxic to reproduction)	☐	[fluid], [quantity]
	Toxic/Irritant	☐	[fluid], [quantity]
	Corrosive	☐	[fluid], [quantity]
	Oxidizing	☐	[fluid], [quantity]
	Flammable/Potentially explosive atmospheres	☐	[fluid], [quantity]
	Dangerous for the environment	☐	[fluid], [quantity]
Non-ionizing radiation Safety	Laser	☐	[laser], [class]
	UV light	☐	
	Magnetic field	☐	[magnetic field] [T]
Workplace	Excessive noise	☒	Background noise ISOLDE hall and PAC spectrometers
	Working outside normal working hours	☒	Shifts are performed according to the ISOLDE schedule.
	Working at height (climbing platforms, etc.)	☐	
	Outdoor activities	☐	The samples are transported form building 170 to building 508.
Fire Safety	Ignition sources	☐	
	Combustible Materials	☐	
	Hot Work (e.g. welding, grinding)	☒	Annealing up to 800 C
Other hazards			